cells

MDPI

Article

Mechanistic Insights into the Adenosine A1 Receptor's Positive Allosteric Modulation for Non-Opioid Analgesics

Tal Weizmann [1], Abigail Pearce [2], Peter Griffin [1], Achille Schild [3], Maren Flaßhoff [3], Philipp Grossenbacher [3], Martin Lochner [3], Christopher A. Reynolds [1], Graham Ladds [2] and Giuseppe Deganutti [1,*]

[1] Centre for Health and Life Sciences, Coventry University, Coventry CV1 5FB, UK
[2] Department of Pharmacology, University of Cambridge, Tennis Court Road, Cambridge CB2 1PD, UK
[3] Institute of Biochemistry and Molecular Medicine, University of Bern, 3012 Bern, Switzerland
* Correspondence: ad5288@coventry.ac.uk

Abstract: The adenosine A1 receptor (A_1R) is a promising target for pain treatment. However, the development of therapeutic agonists is hampered by adverse effects, mainly including sedation, bradycardia, hypotension, or respiratory depression. Recently discovered molecules able to overcome this impediment are the positive allosteric modulator MIPS521 and the A1R-selective agonist BnOCPA, which are both potent and powerful analgesics with fewer side effects. While BnOCPA directly activates the A_1R from the canonical orthosteric site, MIPS521 binds to an allosteric site, acting in concert with orthosteric adenosine and tuning its pharmacology. Given their overlapping profile in pain models but distinct mechanisms of action, we combined pharmacology and microsecond molecular dynamics simulations to address MIPS521 and BnOCPA activity and their reciprocal influence when bound to the A1R. We show that MIPS521 changes adenosine and BnOCPA G protein selectivity in opposite ways and propose a structural model where TM7 dynamics are differently affected and involved in the G protein preferences of adenosine and BnOCPA.

Keywords: adenosine A1 receptor; BnOCPA; MIPS521; non-opioid analgesia; GPCRs

Citation: Weizmann, T.; Pearce, A.; Griffin, P.; Schild, A.; Flaßhoff, M.; Grossenbacher, P.; Lochner, M.; Reynolds, C.A.; Ladds, G.; Deganutti, G. Mechanistic Insights into the Adenosine A1 Receptor's Positive Allosteric Modulation for Non-Opioid Analgesics. *Cells* **2024**, *13*, 2121. https://doi.org/10.3390/cells13242121

Academic Editor: Trevor W. Stone

Received: 8 November 2024
Revised: 16 December 2024
Accepted: 19 December 2024
Published: 21 December 2024

1. Introduction

The adenosine A1 receptor (A_1R) is highly expressed in the brain cortex, cerebellum, and dorsal horn of the spinal cord [1], where adenosine mediates pain perception by modulating opioid neurotransmitter release [2,3]. It is, therefore, considered an emerging non-opioid target for novel painkillers [4]. However, the A_1R is also present in the autonomic or somatic peripheral nervous systems, where its activation produces sedation, bradycardia, hypotension, and cardiorespiratory depression [5–7]. For this reason, it was considered undruggable until the recent discovery of the A_1R agonist benzyloxycyclopentyladenosine (BnOCPA, Figures 1a and S1) [8] and the A_1R allosteric modulator [2-amino-4-(3,5-bis(trifluoromethyl)phenyl)thiophen-3-yl)(4-chlorophenyl)methanone] MIPS521 [9] (Figure 1a).

Allosteric modulation is the regulation of a protein's activity through the binding of an effector molecule at a specific site on the protein, known as the allosteric site, which is distinct from the orthosteric (main) one [10]. This ternary interaction alters the protein's conformation, thereby modulating its function. Allosteric modulators can either enhance (positive allosteric modulators—PAMs) or inhibit (negative allosteric modulators—NAMs) the activity of the protein. BnOCPA and MIPS521 have divergent action mechanisms but overlapping analgesic effects in vivo. BnOCPA's direct action is orthosterically exerted through the preferential activation by the A_1R of the subtype G_{ob} among the six $G_{\alpha i/o}$ proteins; the PAM MIPS521 enhances the effect of the endogenous agonist adenosine from a membrane-exposed allosteric binding site (Figure 1b).

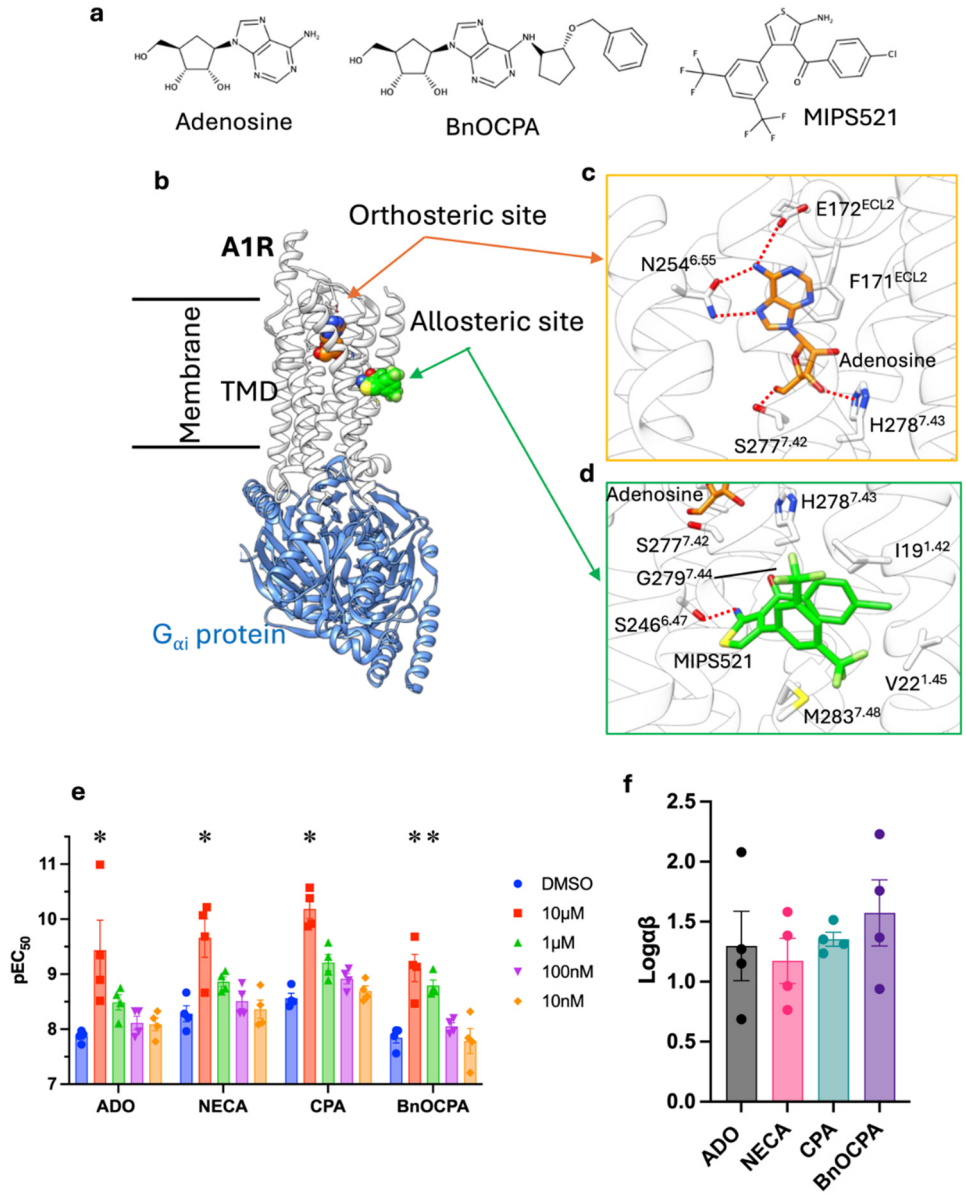

Figure 1. (**a**) Structure of the A_1R ligand simulated in this study: the agonists adenosine and BnOCPA and the positive allosteric modulator MIPS521; (**b**) membrane view of the orthosteric and allosteric binding site of the A_1R (white ribbon) bound to the $G_{\alpha i}$ protein (blue ribbon); (**c**,**d**) detailed binding mode of adenosine (orange) and MIPS521 (green) within their respective binding sites; (**e**) cAMP assay pEC50 of the A_1R agonists CPA, BnOCPA, adenosine (ADO) and NECA at increasing concentrations of MIPS521 (10 nM, orange; 100 nM, purple; 1 μM, green, *: $p = 0.0042$ for BnOCPA; 10 μM, red, *: $p < 0.0001$ for all the agonists tested). (**f**) MIPS allosteric operator Log$\alpha\beta$ measured for CPA (cyan), BnOCPA (purple), ADO (grey), and NECA (pink).

Like the other class A G protein-coupled receptors (GPCRs), the A_1R spans the cells' plasma membrane seven times (transmembrane helices 1–7, TM1–7) and presents three intracellular loops (ICLs) and three extracellular loops (ECLs), which are critical for ligand binding [11–13]. The orthosteric site, located within the extracellular end of the transmembrane domain (TMD), stabilises the agonist binding mode thanks to five hydrogen bonds formed by $N254^{6.55}$, $E172^{ECL2}$, $T277^{7.42}$, and $H278^{7.43}$ (superscripts refer to the GPCR Ballesteros-Weinstein residue numbering [14]) as well as pi-pi stacking with $F171^{ECL2}$ (Figure 1c). Agonist binding to the A_1R stabilises the receptor in an active state, exposing the intracellular binding site for $G_{\alpha i/o}$ proteins. Several A_1R conserved motifs are involved

in the structural rearrangement upon activation [15], and many of them are located near the allosteric site for PAMs, which is external to the TMD and exposed to the membrane (Figure 1d). The hydrophobic MIPS521 binds to this accessory site through hydrophobic interactions with M283$^{7.48}$, I19$^{1.42}$, and V22$^{1.45}$, and just one (buried) hydrogen bond with S246$^{6.47}$. Contacts are also formed with G279$^{7.44}$, which is the main player for TM7 flexibility [16].

BnOCPA's signalling dissection has demonstrated that its ability to inhibit excitatory synaptic transmission without causing neuronal membrane hyperpolarisation is due to its propensity to couple to G_{ob} [8]. G_{ob} signalling activated by BnOCPA was validated as paramount for avoiding the depression of heart rate, blood pressure, or respiration in urethane-anaesthetised, spontaneously breathing adult rats. However, whether MIPS521 produces analgesia by switching adenosine selectivity towards G_{ob} intracellular pathways is not known. It is also unknown whether MIPS521 can further enhance BnOCPA's unique signalling profile. In this work, we examined how these remarkable A_1R ligands, BnOCPA and MIPS521, influence each other and what the structural bases are for their reciprocal interaction. We show that the dynamic of the A_1R in complexes with BnOCPA or adenosine is differently affected by MIPS521 and suggest that TM7 is particularly important for transmitting BnOCPA's chemical signal.

2. Materials and Methods

2.1. Chemical Synthesis

BnOCPA and MIPS521 Synthesis

The A_1R agonist BnOCPA was synthesised according to our previously published procedure [17]. MIPS521 was synthesised according to the literature [18]. Both isolated compounds were unambiguously confirmed by nuclear magnetic resonance (NMR) and mass spectroscopy (MS) analyses and had a chemical purity of >95% according to high-performance liquid chromatography (HPLC) analysis.

2.2. Pharmacology

2.2.1. cAMP Accumulation Assays

The measurement of ligand-induced cyclic adenosine monophosphate (cAMP) accumulation was performed in CHO-K1 cells stably expressing the A_1R. Cells were cultured in F12 media supplemented with 10% foetal bovine serum (FBS), 1% antibiotic-antimycotic (AA) solution, and 600 µg/mL G418. Cells were maintained at 37 °C in 5% CO_2. cAMP was measured using the LANCE*ultra* cAMP detection kit (Revvity) as per the manufacturer's guidance and as previously described [8]. Cells were stimulated with adenosine, BnOCPA, cyclopentyladenosine (CPA), or 5-(N-ethylcarboxamido)adenosine (NECA) over the concentration range of 1 µM to 1 pM in the absence or presence of 10 µM–1 nM MIPS521. Cells were stimulated for 30 min, and plates were read using a Mithras LB 940 multimode microplate reader.

2.2.2. TRUPATH G Protein Dissociation Assay

$G_{o\alpha}$ protein dissociation was measured using the TRUPATH biosensor platform [19], as described previously [8]. HEK293T cells, grown in Dulbecco's modified Eagle medium (DMEM)/F12 Glutamax supplemented with 10% FBS and 1% AA solution, were transfected with 400 ng each of A_1R, Gαo-Renilla Luciferase (Rluc)8, Gβ3, and Gγ8. After 24 h, cells were seeded at 50,000 cells per well of a white 96-well plate and assayed after another 24 h. Cells were stimulated with adenosine and BnOCPA over the concentration range of 10 µM to 10 pM in the absence or presence of 10 nM MIPS521. Plates were read for 15 min using a BRET2 module of a PheraStar at 60-s intervals. The BRET2 ratio after 10 min was used to calculate potency parameters.

2.2.3. Data Analysis

Data were fitted using GraphPad Prism 10, the 3-parameter logistic equation, and the operational model of allosterism [20].

2.3. Computational Molecular Modelling

2.3.1. Force Field and Ligands' Parameters

The CHARMM36 [21,22]/CGenFF 3.0.1 [23–25] force field combination was employed in this work. Initial adenosine and MIPS521 (Figure 1a) force field topology and parameter files were obtained from the ParamChem webserver [23]. Force field parameters for BnOCPA were reported previously [8].

2.3.2. System Preparation for Molecular Dynamics (MD) Simulations

The active state of the A_1R in complex with adenosine and MIPS521 was retrieved from the Protein Data Bank database [26], entry 7LD3 [9]. The modelling of the A_1R's missing intracellular loop 3 (ICL3) and $G_{\alpha i2}$ alpha-helical domain (AHD) was not attempted. In our previous work [8], four different orientations of BnOCPA benzyloxy moiety were sampled (Figure S1). In this work, we started the simulations with BnOCPA in mode C, where the benzyloxy moiety was oriented towards $Y271^{7.36}$ and inserted it into the A_1R (7LD3) by superimposition with the A_1R from our previous work.

Six different systems were prepared (Table 1): (*i*) two quaternary complexes were formed by agonists (adenosine or BnOCPA), A_1R, MIPS521, and G_{i2}; (*ii*) the same as (i) but omitting G_{i2}; and (*iii*) the same as (i) but omitting MIPS521.

Table 1. Summary of the MD simulations performed.

Complex Components	Coordinates Source	# Replicas (Total MD Sampling)/μs	Initial System Dimensions/Å
A_1R Adenosine MIPS521 $G_{\alpha i2}$	PDB 7LD3 PDB 7LD3 PDB 7LD3 PDB 7LD3	3 × 1 (3)	111 × 101 × 156 167,339 atoms
A_1R Adenosine $G_{\alpha i2}$	PDB 7LD3 PDB 7LD3 PDB 7LD3	3 × 1 (3)	111 × 101 × 156 167,300 atoms
A_1R Adenosine MIPS521	PDB 7LD3 PDB 7LD3 PDB 7LD3	3 × 1 (3)	81 × 81 × 106 64,639 atoms
A_1R BnOCPA MIPS521 $G_{\alpha i2}$	PDB 7LD3 Mode C (Ref [8]) PDB 7LD3 PDB 7LD3	3 × 1 (3)	111 × 101 × 156 167,500 atoms
A_1R BnOCPA $G_{\alpha i2}$	PDB 7LD3 Mode C (Ref [8]) PDB 7LD3	3 × 1 (3)	111 × 101 × 156 167,461 atoms
A1R BnOCPA MIPS521	PDB 7LD3 Mode C (Ref [8]) PDB 7LD3	3 × 1 (3)	81 × 81 × 106 64,797 atoms

Hydrogen atoms were added using pdb2pqr [27] and propka [28] software (considering a simulated pH of 7.0); the protonation of titratable side chains was checked by visual inspection. The resulting receptors were separately inserted in a 1-palmitoyl-2-oleyl-sn-glycerol-3-phosphocholine (POPC) bilayer (previously built using the VMD Membrane Builder plugin 1.1, Membrane Plugin, Version 1.1. at http://www.ks.uiuc.edu/Research/vmd/plugins/membrane/ accessed on 11 November 2023), through an insertion method [29]. The receptor orientation was obtained by superposing the coordinates on the

corresponding structure retrieved from the OPM database [30]. Lipids overlapping the receptor transmembrane helical bundle were removed, and TIP3P water molecules [31] were added to the simulation box employing the VMD Solvate plugin 1.5 (Solvate Plugin, Version 1.5. at http://www.ks.uiuc.edu/Research/vmd/plugins/solvate/ accessed on 11 November 2023). Finally, overall charge neutrality was reached by adding Na^+/Cl^- counter ions up to the final concentration of 0.150 M), using the VMD Autoionize plugin 1.3 (Autoionize Plugin, Version 1.3. at http://www.ks.uiuc.edu/Research/vmd/plugins/autoionize/ accessed on 11 November 2023).

2.3.3. System Equilibration and Molecular Dynamics Settings

The MD engine ACEMD3 [32] was employed for both the equilibration and productive simulations. The equilibration was achieved in isothermal–isobaric conditions (NPT) using the Berendsen barostat [33] (target pressure 1 atm) and the Langevin thermostat [34] (target temperature 300 K) with low damping at 1 ps^{-1} and an integration time step of 2 fs. An initial 1 kcal mol^{-1} $Å^{-2}$ restraint was applied to protein, ligands, and lipid phosphorus atoms. Restraints not involving the ligands were gradually released at 4 ns (phosphorus atoms), 60 ns (protein atoms other than Cα atoms), and 80 ns (protein Cαatoms). A further 20 ns (in the absence of the G_{i2} protein) or 40 ns (in the presence of the G_{i2} protein) of equilibration were run with restraints applied only on ligand atoms. Productive trajectories (Table 1) were computed with an integration time step of 4 fs in the canonical ensemble (NVT). The target temperature was set at 300 K, using a thermostat damping of 0.1 ps^{-1}; the M-SHAKE algorithm [35,36] was employed to constrain the bond lengths involving hydrogen atoms. The cut-off distance for electrostatic interactions was set at 9 Å, with a switching function applied beyond 7.5 Å. Long-range Coulomb interactions were handled using the particle mesh Ewald summation method (PME) [37] by setting the mesh spacing to 1.0 Å.

2.3.4. Molecular Dynamics Trajectories: Analysis

Root mean square deviations (RMSDs) and root mean square fluctuations (RMSFs) were computed using VMD [38] and dihedral angles with MDAnalysis [39]. Interatomic contacts were detected using the GetContacts scripts tool (https://getcontacts.github.io accessed on 4 June 2022). Contacts and hydrogen bond persistency were quantified as the percentage of frames (over all the frames obtained by merging the different replicas) in which protein residues formed contacts or hydrogen bonds with the ligand.

For the network analysis, the three replicas simulated for each complex were merged (3 µs for each system). Network and community analyses [40] (code available at http://faculty.scs.illinois.edu/schulten/software/networkTools/index.html accessed on 21 March 2024) were performed within the VMD environment, considering the Cα atoms of A_1R as nodes. A network was formed by an ensemble of nodes interconnected by edges. Edges connected pairs of (non-consecutive) nodes if the corresponding residues were in contact (within 4.5 Å) for at least 75% of the frames. The resulting dynamical network was weighted by considering the probability w_{ij} of information transfer across the edge connecting two nodes *I* and *j*, which were calculated using the following equation:

$$W_{ij} = -\log(|C_{ij}|)$$

where $|C_{ij}|$ measures the correlation values of motion between the two residues during the simulation (Figure S2).

2.4. G Protein-Coupled Receptor Numbering System

Throughout the manuscript, the Ballesteros-Weinstein residue numbering system for GPCRs [14] was adopted.

3. Results

3.1. MIPS521 Similarly Enhances the Potency of Different A_1R Agonists

In a cAMP inhibition assay, MIPS521 acts as an agonist of the A_1R, consistent with previous observations [9]. We sought to examine its effects against different A_1R orthosteric agonists: the non-selective adenosine and N-ethylcarboxamindoadenosine (NECA), and the A_1R selective agonists N^6-cyclopentyladenosine (CPA) and BnOCPA. MIPS521, tested across the concentration range of 10 nM to 10 µM, potentiated all four orthosteric agonists to similar extents (Figures 1e and S3, Table 2). The cooperativity operator Log$\alpha\beta$ [41], incorporating allosteric effects on affinity (α) and efficacy (β), computed for the four agonists resulted in values between 1.17 and 1.57 (Figure 1f, Table 2), confirming a comparable effect of MIPS512 on all the agonists tested.

Table 2. pEC_{50} and Log$\alpha\beta$ values show comparable allosteric modulation for all orthosteric agonists tested. Values calculated from cAMP accumulation assays are reported as the mean ± SEM of $n = 4$ replicates. Significance from DMSO was determined through a Two-Way ANOVA with Dunnett's post hoc test for multiple comparisons.

Agonist	DMSO	10 µM	1 µM	100 nM	10 nM	Log$\alpha\beta$
Adenosine	7.85 ± 0.07	9.46 ± 0.55 *	8.51 ± 0.14	8.12 ± 0.12	8.09 ± 0.12	1.30 ± 0.29
NECA	8.31 ± 0.17	9.61 ± 0.32 *	8.69 ± 0.09	8.51 ± 0.14	8.36 ± 0.17	1.17 ± 0.19
CPA	8.56 ± 0.09	10.22 ± 0.14 *	9.22 ± 0.15	8.92 ± 0.09	8.69 ± 0.09	1.35 ± 0.06
BnOCPA	7.76 ± 0.13	9.34 ± 0.36 *	8.82 ± 0.10 *	8.05 ± 0.07	7.79 ± 0.23	1.57 ± 0.28

* $p < 0.05$.

3.2. MIPS521 Requires $G_{i/o}$ for A_1R Stable Binding

To retrieve structural insights into the allosteric mechanism putatively triggered by MIPS521 on adenosine and BnOCPA, six different systems were subjected to MD simulations (Table 1): (*i*) two quaternary complexes formed by an agonist (adenosine or BnOCPA), A_1R, MIPS521 and G_{i2}; (*ii*) the same as in (i) but omitting MIPS521; or (*iii*) the as in (i) but omitting G_{i2}.

During MD simulations of MIPS521 in a ternary complex with the A_1R and adenosine (Figure S4a), MIPS521 remained bound to the A_1R in two out of three replicas and dissociated from the receptor in Replica 3 after 550 ns. This latter MIPS521's unstable behaviour was observed in a ternary complex with the A_1R and BnOCPA (Figure S4b), where MIPS521 either transiently (Replicas 1 and 2) or permanently (Replica 3) unbound from the A_1R. On the other hand, in a quaternary complex with the A_1R, G_{i2}, and either adenosine or BnOCPA (Figure S4c,d), MIPS521 remained stably bound to the A_1R (RMSD 2.32 ± 0.87 Å and 2.50 ± 1.72 Å, respectively) except for transient conformational rearrangements highlighted by RMSD values of 6–8 Å. These computational results suggest that MIPS521 binding is allosterically favoured by $G_{i/o}$, thanks to the stabilisation provided by TM6 in the active conformation, which is necessary for shaping the MIPS521 membrane-facing binding site (Figure 1d).

3.3. BnOCPA Binding Mode Is Affected by G_{i2} and MIPS512 Through TM7 Dynamics

Focusing on the simulated agonists, adenosine experienced similar fluctuations within the A_1R orthosteric site in a ternary complex with the A_1R and MIPS521 (Figure S5a) or with the A_1R and G_{i2} (Figure S5c) (RMSD 1.46 ± 0.49 Å and 1.43 ± 0.61 Å, respectively). However, it was stabilised in the quaternary complex with A_1R, MIPS521 and G_{i2} (1.03 ± 0.41 Å, Figure S5e). BnOCPA in a ternary complex with the A_1R and MIPS521 (Figure S5b) remained stably bound in the initial conformation during two replicas out of three, with Replica 3 characterised by a rotation of the benzyloxy-cyclopentyl group from mode C to modes A or B (Figure S1) after 0.5 µs. Interestingly, BnOCPA's conformational rearrangements from mode C to modes A and B were sampled in all three replicas per-

formed on the ternary complex comprising A_1R and G_{i2} (i.e., without MIPS512) within 0.8 µs (Figure S5d, Video S1) but not when MIPS521 was present in the quaternary complex (Figure S5f, Video S1). In this latter stable configuration, the RMSD of BnOCPA remained stably low (1.54 ± 0.53 Å), and the agonist benzyloxy-cyclopentyl group was stably oriented in mode C (Figure S1). This confirms that the allosteric effect of MIPS521 on adenosine likely depends on the presence of G_{i2} and whether G_{i2} alone or with MIPS521 differently influences BnOCPA's orthosteric dynamics.

To investigate the structural bases involved in the different allosteric effects exerted by G_{i2} alone and in the co-presence of MIPS521, we analysed the flexibility of the A_1R Cα during the MD simulations in complex with adenosine or BnOCPA in these two divergent situations (Figure 2a–d). Regardless of the agonist bound, a comparison between A_1R backbone flexibility with and without MIPS521 showed the stabilisation of the intracellular end of TM6 and the extracellular loop 2 (ECL2) due to PAM binding. This is consistent with the MIPS521 binding site partially involving TM6 and, therefore, a reduction in TM6 and the fluctuation favoured by the hydrogen bond with $S246^{6.47}$. An ECL2 stabilisation triggered by MIPS521 was also observed by Solano et al. by employing enhanced sampling MD simulations [16]. A difference, evident only in the BnOCPA-bound A_1R without MIPS521, is represented by the higher flexibility in TM7 (residues $G279^{7.44}$ and $N280^{7.45}$) and TM2 (e.g., $N70^{2.65}$) (Figure 2c, Video S1). The binding of MIPS521 to the A_1R in complex with BnOCPA and G_{i2} (Figure 2d) had the effect of reducing the fluctuations of $G279^{7.44}$ and $N280^{7.45}$. This was likely due to direct interactions with TM7 and TM2, caused by an allosteric effect that could involve the stabilisation of BnOCPA in binding mode C (Video S1).

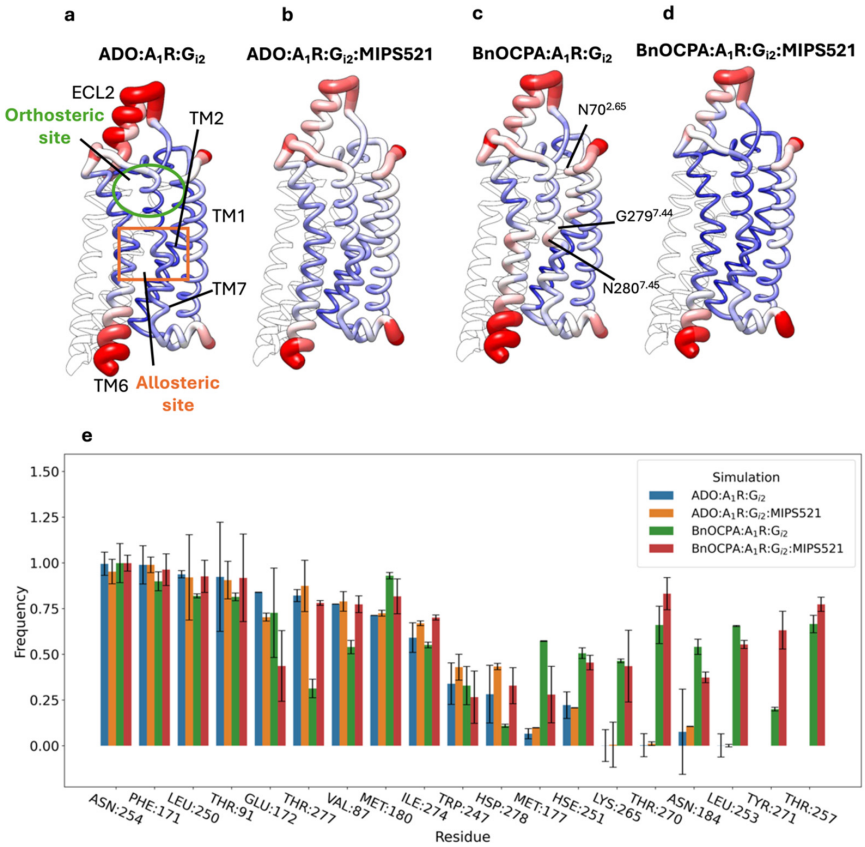

Figure 2. (**a**–**d**) A_1R Cα root mean square fluctuations (RMSFs) plotted on the receptor backbone, colour-coded, and with ribbon thickness proportional to the RMSF value for (**a**) ADO:A_1R:G_{i2}, (**b**) ADO:A_1R:G_{i2}:MIPS521, (**c**) BnOCPA:A_1R:G_{i2}, (**d**) BnOCPA:A_1R:G_{i2}:MIPS521; the orange rectangle in (**a**) indicates the MIPS521 binding site position. (**e**) Contacts between the A_1R and adenosine or BnOCPA in a ternary or quaternary complex with G_{i2} and MIPS521.

The side chain conformational analysis of the residues connecting MIPS521 and the agonist binding site revealed a divergent rotameric distribution of $T277^{7.42}$ and $H278^{7.43}$, both pivotal for A_1R activation [42], whether MIPS521 was co-present with G_{i2} or absent (Figure S6b,d). The conformational shift of $T277^{7.42}$ and $H278^{7.43}$ upon MIPS521 binding was paralleled by increased interactions with BnOCPA, which was particularly evident for $T277^{7.42}$ (Figure 2e). No significant differences in side chain conformation or interactions were observed for adenosine (Figures 2e and S6a,c).

Taken together, these results suggest a structural communication between the MIPS521 and BnOCPA binding sites that involve TM7, not parallel to the endogenous agonist adenosine.

3.4. G_{i2} and MIPS512 Favour Different Interactions Within the BnOCPA-Bound A_1R

Given the role of TM7 suggested by the previous analysis, we focused on A_1R intramolecular interactions involving TMD residues at the level of the MIPS521 binding site, particularly near the conserved residues $D55^{2.50}$ and $N284^{7.49}$, which are involved in receptor activation [42]. When the adenosine was bound to A_1R, either in a ternary complex with G_{i2} or a quaternary complex with MIPS521 as well, no significant changes in contacts were evident for $N280^{7.45}$, $S281^{7.46}$, or $N284^{7.49}$ (Figure 3a). Significant increases in interactions between TM7 and TM2 or TM1 (i.e., $N280^{7.45}$-$W247^{6.48}$, $S281^{7.46}$-$D55^{2.50}$, $S281^{6.46}$-$N27^{1.50}$, and $N280^{7.45}$-$N284^{7.49}$) were observed with BnOCPA bound to A_1R:G_{i2}:MIPS521 compared to A_1R:G_{i2} (Figure 3a), paralleled by a reduction in intrahelical TM7 contacts (i.e., $L276^{7.41}$-$N280^{7.45}$ and $S281^{7.46}$-$N284^{7.49}$) suggesting the strengthening of the intramolecular interactions between TM7 and TM2 or TM1 due to the PAM.

A network analysis was performed to pinpoint the A_1R residues involved in the flow of structural information through the receptor's TM7 under the different simulated conditions (Figure 3b–e). Interestingly, the presence of MIPS521 bound to A_1R, in turn, and in complex with adenosine, concentrated the structural information in the middle of TM7 and involved $F275^{7.40}$, $H278^{7.43}$, and $S281^{7.46}$, in addition to $G279^{7.44}$ (Figure 3c), compared to the sparse configuration in the absence of MIPS521 (Figure 3b). Contrarily, the TM7 of BnOCPA-bound A_1R was deactivated by MIPS521, as shown by the marked reduction in structural information through TM7 (Figure 3d,e). In the latter case, BnOCPA was able to trigger a dense and extended network of correlated movement involving the TM7 of the A_1R bound to G_{i2} in the absence of MIPS521 (Figure 3d), which instead turned off the structural communication in the extracellular half of the helix, de facto isolating the orthosteric binding site from the intracellular side of TM7 (Figure 3e).

To assess any difference in the G protein subtype activation by MIPS521, possibly due to the intramolecular interaction network stabilised by MIPS521 and BnOCPA, we performed TRUPATH experiments detecting $G_{\beta\gamma}$ and its dissociation from $G_{oa\alpha}$ or $G_{ob\alpha}$. A significant enhancement of the G_{ob} activation by adenosine (Figures 3f and S7, Table 3) and G_{oa} activation by BnOCPA (Figures 3g and S7, Table 3**)** was detected at 10 nM of MIPS521. Consistent with the different interactions in the network pinpointed by MD simulations, these results show a divergent effect of MIPS521 on the $G_{i/o}$ protein subtype's selectivity of two agonists. BnOCPA displayed a loss of G_{ob} selectivity due to MIPS512, whereas adenosine gained G_{ob} selectivity.

Table 3. pEC50 values for Gαo protein dissociation in response to the stimulation with ADO or BnOCPA in the presence of either 0.1% DMSO or 10 nM MIPS521. Mean values are reported as the ± SEM of n individual experiments, where n is between 4 and 5. The significance of DMSO-treated cells was determined using a Two-Way ANOVA.

	G_{oa}		**G_{ob}**	
Agonist	**DMSO**	**10nM MIPS521**	**DMSO**	**10nM MIPS521**
Adenosine	7.63 ± 0.30	8.33 ± 0.30	7.09 ± 0.38	8.66 ± 0.46 *
BnOCPA	7.40 ± 0.11	7.92 ± 0.12 *	7.81 ± 0.08	7.65 ± 0.13

* $p < 0.05$.

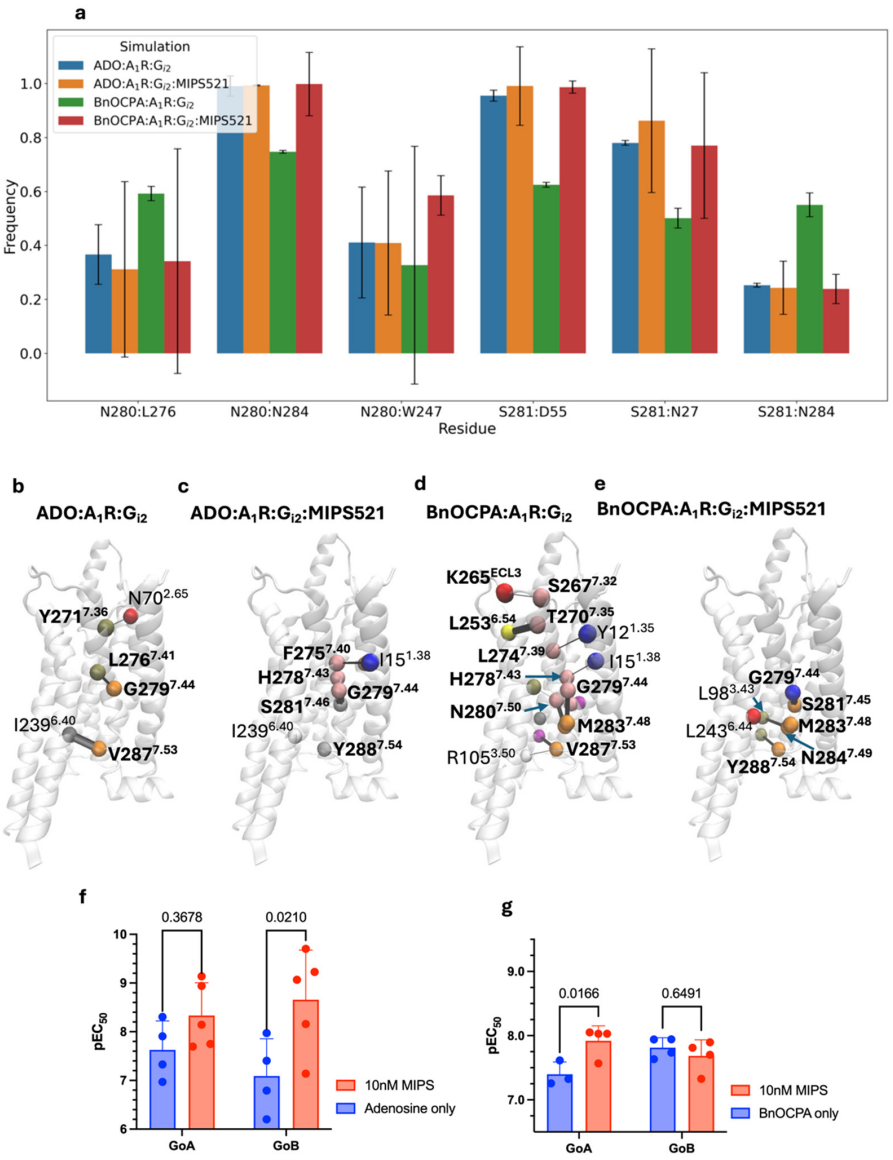

Figure 3. (**a**) Intramolecular contacts between the A_1R residues on TM7 and TM1 or TM2 during MD simulations of the A_1R in a ternary complex with G_{i2} and adenosine or BnOCPA or in a ternary or quaternary complex with G_{i2} and MIPS521; standard deviations from 3 replicas are reported. (**b**–**e**) Network analysis of TM7 during MD simulations of the A_1R in ternary complex with G_{i2} and adenosine or BnOCPA, or a ternary or quaternary complex with G_{i2} and MIPS521; Cα carbons are shown as van der Waals spheres (nodes) and node edges as black lines of thickness proportional to the structural information computed. (**f**,**g**) G_{oa} and G_{ob} activation of TRUPATH pEC50 for adenosine and BnOCPA.

4. Discussion

In the present work, we first showed that adenosine and its derivatives, CPA, BnOCPA, and NECA, are consistently enhanced by MIPS521, as demonstrated by the increase in pEC_{50} and the similar value of the allosteric operator Logαβ. Microsecond MD simulations of the A_1R in complex with adenosine or BnOCPA, with or without G_{i2} or MIPS521, indicated that the PAM requires an active state of TM6 conformation stabilised by G_{i2} to bind to the receptor's external binding site. These results, in agreement with previously reported Gaussian-accelerated MD simulations by Miao and co-workers [9], also showed that MIPS521 binding reciprocally affects TM6 flexibility when A_1R engages G_{i2}, likely stabilising the G protein [9]. Given that this reciprocal allosteric communication between

the intracellular effector and the PAM is observed for both adenosine and BnOCPA, we hypothesise that the TM6 stabilisation can play a role in the generic, unselective activation of any Gi/o protein, which would explain the common increase in cAMP inhibition for both adenosine and BnOCPA.

In the absence of MIPS521, the BnOCPA:A_1R:G_{i2} complex displayed high TM7 flexibility that was not paralleled by adenosine in the same conditions. The high intracellular plasticity of TM7 was also evident in our previous computational characterisation of BnOCPA [8] in the binary complex with A_1R (i.e., without Gi2 and in the absence of MIPS521). The hypothesis that TM7 is pivotal for the unique pharmacological profile of BnOCPA on that occasion [8] was partially supported by the mutagenesis of the A_1R residues located at the TM7/H8 interface level. Indeed, the mutation of R291$^{7.56}$, I292$^{8.47}$, Q293$^{8.48}$, and K294$^{8.49}$ to alanine differentially affected agonist efficacy against stimulated cAMP production. Our new MD-based results strengthen the hypothesise that a direct effect of MIPS521 can be had on TM7 at the level of the A_1R residues G279$^{7.44}$ and N280$^{7.45}$ that are transmitted to the orthosteric binding site through TM7, with the impact of altering T277$^{7.42}$ and H278$^{7.43}$ side chain dynamics and stabilising the BnOCPA binding mode in the C orientation. The divergent structural response of TM7 to MIPS521 when adenosine or BnOCPA were bound to the receptor might underlie the opposite G_{oa} and G_{ob} selectivity enhancement produced by the PAM. This can be framed in the probe-dependency of allosteric modulation, where the response of a receptor to an allosteric modulator varies based on the nature of the orthosteric ligand. In GPCRs, probe-dependency is often observed because the orthosteric ligands stabilise different receptor states, affecting how PAMs influence receptor activation and signal transduction [43]. MIPS521, reducing the efficacy of BnOCPA by activating G_{ob}, would not represent an obstacle to developing A_1R agonist painkillers because they can independently stimulate the G_{ob} pathway (Figure 4), as demonstrated by BnOCPA. On the other hand, MIPS (and related PAMs) depend on endogenous agonist adenosine rather than xenobiotic compounds for producing in vivo analgesia.

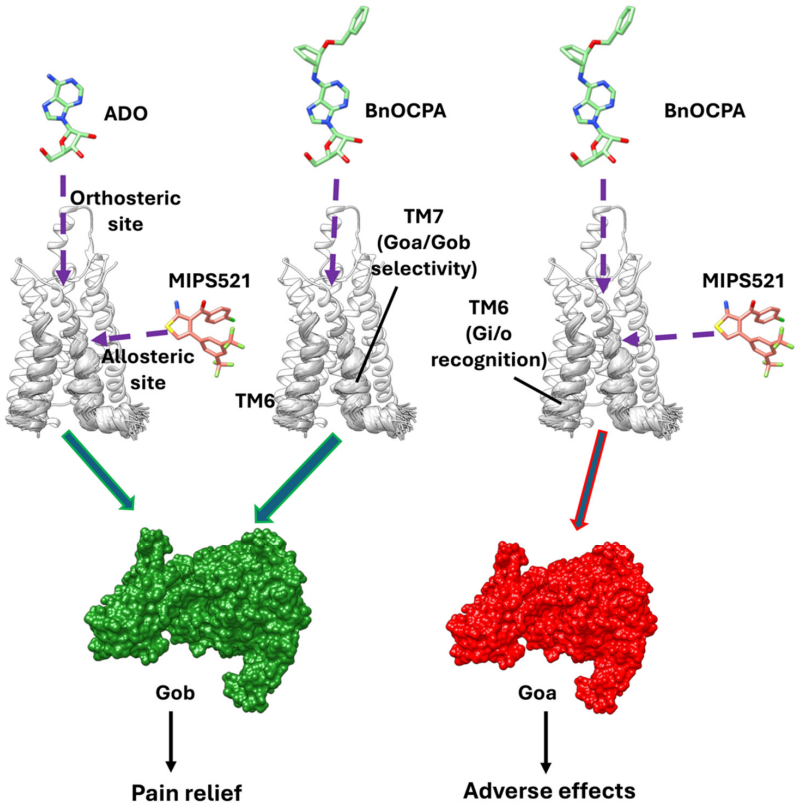

Figure 4. MIPS521 probe-dependent effect and proposed model of G_{ob} selectivity mediated by TM7. Adenosine (ADO) and MIPS521 favour the A_1R selectivity towards G_{ob}, in analogy with BnOCPA alone.

MIPS521 shifts A_1R signalling towards G_{oa}, potentially producing undesired effects. TM7 dynamics, differently affected by adenosine and BnOCPA, are proposed to be crucial for MIPS521 probe-dependent signalling and, hence, for G_{oa}/G_{ob} selectivity.

Importantly, the α subunit, pivotal for the trimeric G protein coupling [44] of G_{oa} and G_{ob}, differs in just 19 residues, none of which are part of the main interface engaging the A_1R. We propose that the selectivity towards one or the other of these two $G_{i/o}$ isoforms is due to a concerted mechanism involving the receptor subdomains TM6 and TM7.

5. Conclusions

Understanding the structural bases for agonist-specific $G_{i/o}$ activation in a dynamic molecular context could speed up the long-awaited rational development of novel non-opioid analgesics based on purinergic signalling. Here, we propose new molecular details of the A_1R activation by BnOCPA and its modulation by MIPS521, which are both considered promising lead compounds. We previously demonstrated that the analgesic effect of BnOCPA is due to G_{ob} selectivity. Here, we report that MIPS512 in vivo analgesia can be due to the sensitisation of adenosine towards $G_{ob.}$ However, the reciprocal structural communication through TM7, as suggested by our computational modelling, between BnOCPA and MIPS521 could reduce BnOCPA potency towards G_{ob} and, in turn, its efficacy as an analgesic. Our key finding that the A_1R-dependent G_{ob} signalling path activation, which is necessary to mitigate on-target side effects, can be triggered either directly by agonists or allosterically by PAMs broadens the approaches available for rationally designing new and safer non-opioid drugs.

Supplementary Materials: The following supporting information can be downloaded at https://www.mdpi.com/article/10.3390/cells13242121/s1. Video S1: Side-by-side comparison between BnOCPA:A_1R:G_{i2} (ternary complex) and BnOCPA:A_1R:G_{i2} (quaternary complex). Table S1: Summary of cAMP assays**.** Figure S1: BnOCPA orientations**.** Figure S2: (a–d) Correlation of motion between A_1R residues during MD simulations. Figure S3: Dose–response curves for cAMP accumulation assay of the A_1R agonists CPA, BnOCPA, adenosine, and NECA at different MIPS521 concentrations. Figure S4: Root mean square deviations of MIPS521. Figure S5: Root mean square deviations of adenosine or BnOCPA. Figure S6: $T277^{7.42}$ and $T278^{7.43}$ $\chi1$ rotameric distribution during MD simulations. Figure S7: Figure S2. TRUPATH dose–response curves of the A_1R agonists BnOCPA and adenosine in the presence or absence of MIPS521.

Author Contributions: Conceptualisation, G.D., C.A.R. and G.L.; formal analysis, T.W., A.P., A.S., M.F., P.G. (Peter Griffin), M.L., G.D. and P.G. (Philipp Grossenbacher); writing—original draft preparation, G.D.; writing—review and editing T.W., A.P., M.L., C.A.R. and G.D.; visualisation, G.D.; funding acquisition C.A.R., G.L. and G.D. All authors have read and agreed to the published version of the manuscript.

Funding: This research was funded by BBSCR, grant numbers BB/W016974/1 (C.A.R., G.D., T.W., and P.G.) and BB/W014831/1 (G.L. and A.P.). G.L. is also funded by a Royal Society Industry Fellowship (INF/R2/212001).

Institutional Review Board Statement: Not applicable.

Informed Consent Statement: Not applicable.

Data Availability Statement: Data are available upon request.

Conflicts of Interest: The authors declare no conflicts of interest.

Abbreviations

A_1R	adenosine A1 receptor
AA	antibiotic-antimycotic
ADO	adenosine
BnOCPA	benzyloxy-cyclopentyladenosine

BRET	Bioluminescence Resonance Energy Transfer
cAMP	cyclic adenosine monophosphate
CPA	cyclopentyladenosine
DMEM	Dulbecco's modified Eagle medium
ECL	extracellular loop
FBS	foetal bovine serum
GPCRs	G protein-coupled receptor
HPLC	high-performance liquid chromatography
ICL	intracellular loop
MD	molecular dynamics
MIPS521	[2-amino-4-(3:5-bis(trifluoromethyl)phenyl)thiophen-3-yl)(4-chlorophenyl)methanone]
MS	mass spectroscopy
NECA	5-(N-ethylcarboxamido)adenosine
NMR	nuclear magnetic resonance
OPM	orientations of proteins in membranes
PAM	positive allosteric modulator
POPC	1-palmitoyl-2-oleyl-sn-glycerol-3-phosphocholine
RMSD	root mean square deviation
RMSF	root mean square fluctuation
Rluc	Renilla Luciferase
TM	transmembrane helices
TMD	transmembrane domain

References

1. Sawynok, J.; Liu, X.J. Adenosine in the spinal cord and periphery: Release and regulation of pain. *Prog. Neurobiol.* **2003**, *69*, 313–340. [CrossRef]
2. Jung, S.-M.; Peyton, L.; Essa, H.; Choi, D.-S. Adenosine receptors: Emerging non-opioids targets for pain medications. *Neurobiol. Pain.* **2022**, *11*, 100087. [CrossRef] [PubMed]
3. Stone, T.W.; Perkins, M.N. Is adenosine the mediator of opiate action on neuronal firing rate? *Nature* **1979**, *281*, 227–228. [CrossRef]
4. Sawynok, J. Adenosine receptor targets for pain. *Neuroscience* **2016**, *338*, 1–18. [CrossRef]
5. Headrick, J.P.; Ashton, K.J.; Rose'meyer, R.B.; Peart, J.N. Cardiovascular adenosine receptors: Expression, actions and interactions. *Pharmacol. Ther.* **2013**, *140*, 92–111. [CrossRef] [PubMed]
6. Dunwiddie, T.V.; Masino, S.A. The role and regulation of adenosine in the central nervous system. *Annu. Rev. Neurosci.* **2001**, *24*, 31–55. [CrossRef] [PubMed]
7. Borea, P.A.; Gessi, S.; Merighi, S.; Vincenzi, F.; Varani, K. Pharmacology of adenosine receptors: The state of the art. *Physiol. Rev.* **2018**, *98*, 1591–1625. [CrossRef] [PubMed]
8. Wall, M.J.; Hill, E.; Huckstepp, R.; Barkan, K.; Deganutti, G.; Leuenberger, M.; Preti, B.; Winfield, I.; Carvalho, S.; Suchankova, A.; et al. Selective activation of Gαob by an adenosine A1 receptor agonist elicits analgesia without cardiorespiratory depression. *Nat. Commun.* **2022**, *13*, 4150. [CrossRef]
9. Draper-Joyce, C.J.; Bhola, R.; Wang, J.; Bhattarai, A.; Nguyen, A.T.N.; Cowie-Kent, I.; O'Sullivan, K.; Chia, L.Y.; Venugopal, H.; Valant, C.; et al. Positive allosteric mechanisms of adenosine A1 receptor-mediated analgesia. *Nature* **2021**, *597*, 571–576. [CrossRef] [PubMed]
10. Wootten, D.; Christopoulos, A.; Sexton, P.M. Emerging paradigms in GPCR allostery: Implications for drug discovery. *Nat. Rev. Drug Discov.* **2013**, *12*, 630–644. [CrossRef]
11. Wheatley, M.; Wootten, D.; Conner, M.T.; Simms, J.; Kendrick, R.; Logan, R.T.; Poyner, D.R.; Barwell, J. Lifting the lid on GPCRs: The role of extracellular loops. *Br. J. Pharmacol.* **2012**, *165*, 1688–1703. [CrossRef] [PubMed]
12. Peeters, M.C.; van Westen, G.J.P.; Li, Q.; IJzerman, A.P. Importance of the extracellular loops in G protein-coupled receptors for ligand recognition and receptor activation. *Trends Pharmacol. Sci.* **2011**, *32*, 35–42. [CrossRef] [PubMed]
13. Deganutti, G.; Barkan, K.; Preti, B.; Leuenberger, M.; Wall, M.; Frenguelli, B.G.; Lochner, M.; Ladds, G.; Reynolds, C.A. Deciphering the agonist binding mechanism to the adenosine A1 receptor. *ACS Pharmacol. Transl. Sci.* **2021**, *4*, 314–326. [CrossRef]
14. Ballesteros, J.A.; Weinstein, H. [19] Integrated methods for the construction of three-dimensional models and computational probing of structure-function relations in G protein-coupled receptors. In *Receptor Molecular Biology*; Methods in Neurosciences; Elsevier: Amsterdam, The Netherlands, 1995; Volume 25, pp. 366–428.
15. Hauser, A.S.; Kooistra, A.J.; Munk, C.; Heydenreich, F.M.; Veprintsev, D.B.; Bouvier, M.; Babu, M.M.; Gloriam, D.E. GPCR activation mechanisms across classes and macro/microscales. *Nat. Struct. Mol. Biol.* **2021**, *28*, 879–888. [CrossRef] [PubMed]

16. Maria-Solano, M.A.; Choi, S. Dynamic allosteric networks drive adenosine A1 receptor activation and G-protein coupling. *Elife* **2023**, *12*, RP90773. [CrossRef] [PubMed]
17. Knight, A.; Hemmings, J.L.; Winfield, I.; Leuenberger, M.; Frattini, E.; Frenguelli, B.G.; Dowell, S.J.; Lochner, M.; Ladds, G. Discovery of novel adenosine receptor agonists that exhibit subtype selectivity. *J. Med. Chem.* **2016**, *59*, 947–964. [CrossRef] [PubMed]
18. Aurelio, L.; Valant, C.; Flynn, B.L.; Sexton, P.M.; Christopoulos, A.; Scammells, P.J. Allosteric modulators of the adenosine A1 receptor: Synthesis and pharmacological evaluation of 4-substituted 2-amino-3-benzoylthiophenes. *J. Med. Chem.* **2009**, *52*, 4543–4547. [CrossRef]
19. Olsen, R.H.J.; DiBerto, J.F.; English, J.G.; Glaudin, A.M.; Krumm, B.E.; Slocum, S.T.; Che, T.; Gavin, A.C.; McCorvy, J.D.; Roth, B.L.; et al. TRUPATH, an open-source biosensor platform for interrogating the GPCR transducerome. *Nat. Chem. Biol.* **2020**, *16*, 841–849. [CrossRef]
20. Gregory, K.J.; Giraldo, J.; Diao, J.; Christopoulos, A.; Leach, K. Evaluation of Operational Models of Agonism and Allosterism at Receptors with Multiple Orthosteric Binding Sites. *Mol. Pharmacol.* **2020**, *97*, 35–45. [CrossRef]
21. Huang, J.; MacKerell, A.D. CHARMM36 all-atom additive protein force field: Validation based on comparison to NMR data. *J. Comput. Chem.* **2013**, *34*, 2135–2145. [CrossRef] [PubMed]
22. Huang, J.; Rauscher, S.; Nawrocki, G.; Ran, T.; Feig, M.; de Groot, B.L.; Grubmüller, H.; MacKerell, A.D. CHARMM36m: An improved force field for folded and intrinsically disordered proteins. *Nat. Methods* **2017**, *14*, 71–73. [CrossRef]
23. Vanommeslaeghe, K.; MacKerell, A.D. Automation of the CHARMM General Force Field (CGenFF) I: Bond perception and atom typing. *J. Chem. Inf. Model.* **2012**, *52*, 3144–3154. [CrossRef] [PubMed]
24. Vanommeslaeghe, K.; Raman, E.P.; MacKerell, A.D. Automation of the CHARMM General Force Field (CGenFF) II: Assignment of bonded parameters and partial atomic charges. *J. Chem. Inf. Model.* **2012**, *52*, 3155–3168. [CrossRef] [PubMed]
25. Yu, W.; He, X.; Vanommeslaeghe, K.; MacKerell, A.D. Extension of the CHARMM General Force Field to sulfonyl-containing compounds and its utility in biomolecular simulations. *J. Comput. Chem.* **2012**, *33*, 2451–2468. [CrossRef] [PubMed]
26. Berman, H.M.; Westbrook, J.; Feng, Z.; Gilliland, G.; Bhat, T.N.; Weissig, H.; Shindyalov, I.N.; Bourne, P.E. The protein data bank. *Nucleic Acids Res.* **2000**, *28*, 235–242. [CrossRef]
27. Dolinsky, T.J.; Nielsen, J.E.; McCammon, J.A.; Baker, N.A. PDB2PQR: An automated pipeline for the setup of Poisson-Boltzmann electrostatics calculations. *Nucleic Acids Res.* **2004**, *32*, W665–W667. [CrossRef]
28. Olsson, M.H.M.; Søndergaard, C.R.; Rostkowski, M.; Jensen, J.H. PROPKA3: Consistent Treatment of Internal and Surface Residues in Empirical pK Predictions. *J. Chem. Theory Comput.* **2011**, *7*, 525–537. [CrossRef] [PubMed]
29. Sommer, B. Membrane Packing Problems: A short Review on computational Membrane Modeling Methods and Tools. *Comput. Struct. Biotechnol. J.* **2013**, *5*, e201302014. [CrossRef]
30. Lomize, M.A.; Lomize, A.L.; Pogozheva, I.D.; Mosberg, H.I. OPM: Orientations of proteins in membranes database. *Bioinformatics* **2006**, *22*, 623–625. [CrossRef] [PubMed]
31. Jorgensen, W.L.; Chandrasekhar, J.; Madura, J.D.; Impey, R.W.; Klein, M.L. Comparison of simple potential functions for simulating liquid water. *J. Chem. Phys.* **1983**, *79*, 926. [CrossRef]
32. Harvey, M.J.; Giupponi, G.; Fabritiis, G.D. ACEMD: Accelerating Biomolecular Dynamics in the Microsecond Time Scale. *J. Chem. Theory Comput.* **2009**, *5*, 1632–1639. [CrossRef] [PubMed]
33. Berendsen, H.J.C.; Postma, J.P.M.; van Gunsteren, W.F.; DiNola, A.; Haak, J.R. Molecular dynamics with coupling to an external bath. *J. Chem. Phys.* **1984**, *81*, 3684. [CrossRef]
34. Loncharich, R.J.; Brooks, B.R.; Pastor, R.W. Langevin dynamics of peptides: The frictional dependence of isomerization rates of N-acetylalanyl-N′-methylamide. *Biopolymers* **1992**, *32*, 523–535. [CrossRef] [PubMed]
35. Forester, T.R.; Smith, W. SHAKE, rattle, and roll: Efficient constraint algorithms for linked rigid bodies. *J. Comput. Chem.* **1998**, *19*, 102–111. [CrossRef]
36. Kräutler, V.; van Gunsteren, W.F.; Hünenberger, P.H. A fast SHAKE algorithm to solve distance constraint equations for small molecules in molecular dynamics simulations. *J. Comput. Chem.* **2001**, *22*, 501–508. [CrossRef]
37. Essmann, U.; Perera, L.; Berkowitz, M.L.; Darden, T.; Lee, H.; Pedersen, L.G. A smooth particle mesh Ewald method. *J. Chem. Phys.* **1995**, *103*, 8577. [CrossRef]
38. Humphrey, W.; Dalke, A.; Schulten, K. VMD: Visual molecular dynamics. *J. Mol. Graph.* **1996**, *14*, 33–38. [CrossRef]
39. Michaud-Agrawal, N.; Denning, E.J.; Woolf, T.B.; Beckstein, O. MDAnalysis: A toolkit for the analysis of molecular dynamics simulations. *J. Comput. Chem.* **2011**, *32*, 2319–2327. [CrossRef] [PubMed]
40. Sethi, A.; Eargle, J.; Black, A.A.; Luthey-Schulten, Z. Dynamical networks in tRNA:protein complexes. *Proc. Natl. Acad. Sci. USA* **2009**, *106*, 6620–6625. [CrossRef] [PubMed]
41. Johnstone, S.; Albert, J.S. Pharmacological property optimization for allosteric ligands: A medicinal chemistry perspective. *Bioorg. Med. Chem. Lett.* **2017**, *27*, 2239–2258. [CrossRef] [PubMed]
42. Jespers, W.; Schiedel, A.C.; Heitman, L.H.; Cooke, R.M.; Kleene, L.; van Westen, G.J.P.; Gloriam, D.E.; Müller, C.E.; Sotelo, E.; Gutiérrez-de-Terán, H. Structural mapping of adenosine receptor mutations: Ligand binding and signaling mechanisms. *Trends Pharmacol. Sci.* **2018**, *39*, 75–89. [CrossRef] [PubMed]

43. Valant, C.; Felder, C.C.; Sexton, P.M.; Christopoulos, A. Probe dependence in the allosteric modulation of a G protein-coupled receptor: Implications for detection and validation of allosteric ligand effects. *Mol. Pharmacol.* **2012**, *81*, 41–52. [CrossRef] [PubMed]
44. Hauser, A.S.; Avet, C.; Normand, C.; Mancini, A.; Inoue, A.; Bouvier, M.; Gloriam, D.E. Common coupling map advances GPCR-G protein selectivity. *Elife* **2022**, *11*, e74107. [CrossRef] [PubMed]